



HAL
open science

Prediction of outcome using pretreatment 18F-FDG PET/CT and MRI radiomics in locally advanced cervical cancer treated with chemoradiotherapy

François Lucia, Dimitris Visvikis, Marie-Charlotte Desseroit, Omar Miranda, Jean-Pierre Malhaire, Philippe Robin, Olivier Pradier, Mathieu Hatt, Ulrike Schick

► To cite this version:

François Lucia, Dimitris Visvikis, Marie-Charlotte Desseroit, Omar Miranda, Jean-Pierre Malhaire, et al.. Prediction of outcome using pretreatment 18F-FDG PET/CT and MRI radiomics in locally advanced cervical cancer treated with chemoradiotherapy. *European Journal of Nuclear Medicine and Molecular Imaging*, In press. hal-01659241

HAL Id: hal-01659241

<https://hal.science/hal-01659241>

Submitted on 8 Dec 2017

HAL is a multi-disciplinary open access archive for the deposit and dissemination of scientific research documents, whether they are published or not. The documents may come from teaching and research institutions in France or abroad, or from public or private research centers.

L'archive ouverte pluridisciplinaire **HAL**, est destinée au dépôt et à la diffusion de documents scientifiques de niveau recherche, publiés ou non, émanant des établissements d'enseignement et de recherche français ou étrangers, des laboratoires publics ou privés.

Prediction of outcome using pretreatment ¹⁸F-FDG PET/CT and MRI radiomics in locally advanced cervical cancer treated with chemoradiotherapy

François Lucia¹, Dimitris Visvikis², Marie-Charlotte Desseroit², Omar Miranda¹, Jean-Pierre Malhaire¹, Philippe Robin³, Olivier Pradier^{1,2}, Mathieu Hatt^{*2}, Ulrike Schick^{*1,2}

*** equally contributed**

1. Radiation Oncology department, University Hospital, Brest, France

2. LaTIM, INSERM, UMR 1101, University of Brest, ISBAM, UBO, UBL, Brest, France

3. Nuclear Medicine department, University Hospital, Brest, France

Corresponding author: François Lucia

Service de radiothérapie

CHRU Morvan, 2 avenue Foch

29609 Cedex, Brest, France

Tel: +33 6 99 74 03 18

E-mail: francois.lucia@gmail.com

ORCID ID : [0000-0001-7286-1350](https://orcid.org/0000-0001-7286-1350)

Wordcount: ~5100

Disclosure of Conflicts of Interest: No potential conflicts of interest were disclosed.

INTRODUCTION

Cervical cancer (CC) is among the most commonly diagnosed cancers for women, with over 500,000 new cases annually worldwide resulting in over 270,000 deaths [1]. A significant proportion of patients are diagnosed at a locally advanced stage, and are usually treated with pelvic external beam radiotherapy (EBRT) in association with cisplatin-based chemotherapy and subsequent brachytherapy (BT). Although chemoradiotherapy (CRT) has significantly improved loco-regional control (LRC) and outcome, approximately 40% of patients suffer from recurrence and eventually die of disease. Several clinical and histopathological variables have been identified as prognostic factors in CC patients, including International Federation of Gynecology and Obstetrics (FIGO) stage, histology and lymph node (LN) metastases [2]. Nevertheless, clinical outcomes are markedly variable among patients with similar stage, which cannot be explained by differences in clinico-pathological features only [2]. Yet the treatment modality choice is based on conventional FIGO and N staging, without prior knowledge regarding CRT efficacy. A more tailored approach based on pre-treatment prediction of recurrence and LRC may allow choosing the appropriate treatment for patients with more aggressive CC [3].

¹⁸F-fluorodeoxyglucose (FDG) positron emission tomography/computed tomography (PET/CT) and magnetic resonance imaging (MRI) play an essential role in the initial staging, therapeutic strategy [4] and treatment response assessment [5]. Recently, in addition to conventional parameters on FDG PET/CT and MRI used to stage disease, plan treatment and assess response there has been a growing interest in the extraction of quantitative features from medical images, denoted radiomics [6]. Radiomics features are statistical or model-based metrics to quantify tumor intensity, shape and heterogeneity which have been shown to reflect intratumoral histopathological properties [7] and to provide prognostic information in several pathologies [8] including CC [9-13]. Radiomics on pretreatment PET/CT has been shown to predict response to therapy and risk of pelvic recurrence in CC [9, 11, 13] and used to characterize CC lesions from diffusion-weighted MRI (DW-MRI) [12] or dynamic contrast enhancement MRI (DCE-MRI) [10]. However, a radiomics signature from both FDG-PET and MRI associated with the outcome of patients with locally advanced CC (LACC) has not yet been described.

Our goal was to develop and validate such a PET/MRI signature with prognostic value for LRC and disease-free survival (DFS) in patients with LACC (stage IB1 to IVA) and to assess its incremental value with respect to the standard clinical and imaging features.

MATERIALS AND METHODS

Patients

Patients with histologically proven LACC, staged IB1-IVA (FIGO 2009 definition) and treated with definitive curative CRT and subsequent BT from August 2010 to December 2016 (to ensure a minimum follow-up of 6 months) at our institution were included in this retrospective study (table 1). Patients with stage IB1 and IIA1 were only considered for inclusion if they had positive LN.

All patients were required to have pelvic examination, PET/CT imaging and pelvic MRI at diagnosis, and at least 6-month of follow-up. Exclusion criteria were history of previous chemotherapy or RT and/or metastatic disease.

Collected data included age and date of diagnosis, histology, FIGO stage, presence of positive LN on PET/CT, tumor size as measured on MRI, body mass index (BMI), complete blood counts (CBC) before treatment, EBRT and BT dose, date and status at last follow-up. Date and site of recurrence were also collected. Recurrences were considered as local (vaginal and/or cervical), regional (pelvic/para-aortic), or distant (upper abdominal and/or extra-abdominal) [14].

A total of 102 patients were recruited and split into training -patients treated from 08/2010 to 05/2015, n=69 (68%)- and testing -patients treated after 05/2015, n=33 (32%)- sets. All patients provided signed permission for the use of their clinical data for scientific purposes and informed consent for the anonymous publication of data. Institutional Review Board approved this study.

Imaging

PET/CT

The Philips Gemini (Philips Medical Systems, Cleveland, OH) was used for the 6 first patients and the Siemens Biograph (SIEMENS Healthineers Medical Solutions, Knoxville, TN) for the next 96 patients after a scanner replacement. Patients fasted for 4h before acquisition, and the blood glucose level had to be less than 7 mmol/L before injection of 5 MBq/kg of ¹⁸F-FDG. PET acquisitions were carried out approximately 60min after injection. The CT consisted of a 64-slice multidetector-row spiral scanner with a transverse field of view of 700 mm. Standard CT parameters were used: a collimation of 16×1.2 mm², pitch 1, tube voltage of 120 kV, and effective tube current of 80 mA. Routine clinical image reconstruction protocols were used: for the Philips GEMINI, data were reconstructed using the RAMLA 3D (2 iterations, relaxation parameter 0.05) whereas for the Siemens Biograph, images were reconstructed with Fourier rebinning (FORE) followed by OSEM (2 iterations, 8 subsets). In both cases images were corrected for attenuation using the corresponding CT, reconstructed with a 2×2×2 mm³ voxels grid and post-filtered with a 5-mm FWHM 3D Gaussian.

MRI

All MRI studies were performed with a 1.5-T unit (Siemens Medical Solutions, Magnetom Aera, Erlangen, Germany or General Electric, Milwaukee, WI) using a phased-array body coil, 2 weeks before the start of CRT with set image protocols. MRI was performed at least 10 days after cone biopsy to avoid false-positive findings due to post-biopsy inflammation. No patient had an absolute contraindication to the MRI examination. The MRI protocol included high-resolution turbo T2-weighted sequences in the sagittal, axial, and axial oblique (perpendicular to the long axis of the cervix) planes. T1-weighted and T2-weighted axial images were obtained through the pelvis and up to the level of the renal hilum to assess nodal status. The MRI protocol included also axial TSE T2-weighted fat-suppressed and axial oblique and sagittal diffusion-weighted images (DWI) (b values of 0, 400 and 1000) without slices gap. All except two allergic patients (training set) received a 0.1

mmol/kg injection of gadobenate dimeglumine (Multihance; Bracco Diagnostics, Milan, Italy). After 3 min a T1-weighted fat-suppressed sequence (CE-MRI) in the axial and sagittal plane was acquired. MRI sequences are described in more details in the supplemental material table 1.

Treatment

Consortium guidelines were applied to contour the clinical target volume (CTV), the planning target volume (PTV) and organs-at-risk [15]. Treatment consisting of three-dimensional conformal radiotherapy (3D-CRT) (n=59 and n=7 respectively in the training and testing sets) or intensity-modulated photon radiotherapy (IMRT) (n=10 and n=26 respectively in the training and testing sets) delivered using a linear accelerator.

All the patients received pelvic EBRT or extended field RT to the para-aortic area using high energy photons (18 MV), depending on their work-up at a dose of 45–50.4 Gy with standard fractionation. In patients with positive pelvic or para-aortic LN, an image-guided targeted boost was delivered to a dose of 50.4-54 Gy to the involved nodes (12 and 3 patients in training and testing sets, respectively). The week after EBRT, patients received 3-4 fractions of MRI-guided high-dose-rate (HDR) intracavitary brachytherapy every 4 days. The prescribed dose was 7 Gy to the high-risk CTV. No patient experienced delays or breaks in RT because of short-term toxicity (median RT duration, 49 days; range, 47-53 days). All patients received 4-6 cycles of concomitant chemotherapy with weekly cisplatin (40 mg/m²) or carboplatin (AUC 2) in case of renal contraindication.

Follow-up

PET/CT (for all patients with the Siemens Biograph) was performed 3 months after treatment completion in order to assess therapeutic response with PERCIST: patients were classified as having complete metabolic response (CMR), partial metabolic response (PMR), stable metabolic disease (SMD), or progressive metabolic disease (PMD) [16]. Clinical follow-up consisted of physical examination every third month until 2 years after diagnosis, every sixth month up to 5 years, annually thereafter, and was done alternatively by the radiation oncologist and gynaecologist. Follow-up imaging studies consisted of MRI at 3 months after treatment completion and annually until 2 years after treatment completion, CT every 6 months until 2 years after treatment completion and if clinically indicated after, and/or PET/CT if clinically indicated.

Workflow for multimodal radiomics

Our workflow is illustrated in Figure 1.

Segmentation

Only primary tumors, not pathological lymph nodes, were analyzed. The PET and the MRI images were processed independently by a single expert radiation oncologist (F. Lucia). To reduce user-dependency of this step, robust (semi)automated methods were exploited. The metabolically active volumes on PET images were automatically delineated with the fuzzy locally adaptive Bayesian (FLAB) algorithm [17, 18]. The anatomic volumes were also delineated on i) the ADC map derived from DWI-MRI, ii) CE-MRI and iii) T2. Each sequence was segmented independently because of anatomical changes between each sequence acquisition, using a previously validated semi-automatic approach exploiting 3D SlicerTM and the Growcut algorithm [19]. This approach only requires painted strokes on the apparent foreground and background as input (examples are provided in supplemental material, figure 2).

Features extraction

Each tumor was characterized with 92 features extracted from four sets of images: the PET component of PET/CT and the 3 MRI sequences (ADC map from DWI, CE-MRI and T2). Amongst these parameters, 19 shape-based features describe the 3D geometry of the segmented volume (e.g. volume or diameter) and 11 first-order statistics are derived from the histogram of voxel intensities (e.g. PET SUV_{max} or SUV_{mean}). Sixty-two 2nd (25 features) and 3rd (37 features) order textures are based on different matrices capturing the spatial intensity distributions at different scales and were calculated in a single matrix considering all 13 orientations simultaneously [20]. For these, three different image intensity quantization methods [21] were considered: a linear quantization of the histogram into 64 bins (Q_L), histogram equalization into 64 bins (Q_E) or using a variable number of fixed-width bins (of 0.5 SUV for PET and 10 units for T2- and CE- MRI and 10 mm²/s for ADC map) (Q_F). This resulted in 186 different features. In the following these will be denoted as Feature_{Matrix-Quantization}. All features were implemented according to the current version of image biomarkers standardization initiative (IBSI) guidelines [20] and a full list is provided in the supplemental material, table 2. A total of 864 image features (216 per modality) 8 clinical and histopathological parameters (age, FIGO stage, N stage, BMI, histology, white blood cells, platelets, hemoglobin) and 3 treatment parameters (radiotherapy dose, brachytherapy dose and overall treatment time) were included in the statistical analysis (table 1).

Statistical analysis

Training and testing sets characteristics were compared using Macnemar test for qualitative factors and Student test for quantitative factors. Endpoints were DFS and LRC. For the training set, all parameters including usual confounding factors (e.g. volume, clinical variables, etc.) were tested using univariate Cox proportional hazards modeling, for which statistical significance was corrected for multiple testing with the Bonferroni method to reduce false-positive discovery rate [22]. Corrected p-values below α/K ($K=875$ and $\alpha=0.05$, i.e. $p<0.000057$) were considered statistically significant. Cox-regression models with the stepwise method were used for multivariate analysis including only the uncorrelated parameters ($r<0.5$) found significant in the univariate analysis. In addition, correlations between the parameters identified in the multivariate analysis and standard metrics (e.g. volume, FIGO stage, etc.) were checked to avoid simply deriving surrogates of usual variables. The receiver operating characteristic (ROC) curve was used to determine cut-off values of significant parameters according to the Youden index to generate Kaplan-Meier curves for DFS and LRC. Distributions of survival times were compared using the log-rank test. The best features/models were applied to the testing set for a rigorous evaluation of their accuracy for DFS and LRC, avoiding overfitting on a single cohort. Adjusted hazard ratios (HRs) and the corresponding 95% confidence intervals (CI) were calculated. All statistical analyses were performed using MedCalc Statistical Software version 15.8 (MedCalc Software bvba, Ostend, Belgium; <https://www.medcalc.org>; 2015). Our study followed the Transparent Reporting of a multivariable prediction model for Individual Prognosis Or Diagnosis (TRIPOD) guidelines [23]. The checklist can be found in the supplemental material.

RESULTS

Patient and tumor characteristics

The training and testing sets had similar clinical, treatment and histopathological characteristics, except for EBRT modalities (more IMRT in the validation set, $p < 0.0001$), which have no impact on the effectiveness of treatment however, only on its toxicity [24].

Outcome

Training set

After a median follow-up of 36 months (range, 6-79 months), 17 patients (25%) had died. Progression or disease recurrence occurred in 25 patients (36%). Fourteen patients (20%) had an isolated pelvic recurrence and 11 (16%) a distant recurrence (8 with isolated distant recurrence and 3 with both regional and distant recurrence). Post-CRT PET/CT demonstrated 44 CMR, 22 PMR, no SMD, and 3 PMD. Out of 14 patients without LRC 4 had a CMR and 10 a PMR. Out of 11 patients with distant metastases 3 had a CMR, 5 a PMR, and 3 a PMD. 3-year DFS and LRC were 63%, and 78%, respectively.

Testing set

None of the 33 patients had died after a median follow-up of 17 months (range, 6–30 months). Progression/recurrence occurred in 10 patients (30%): 5 (15%) had an isolated pelvic recurrence and 5 (15%) a distant recurrence (3 isolated and 2 with both regional and distant). Post-treatment PET/CT demonstrated 19 CMR, 11 PMR, 1 SMD, and 2 PMD. Out of 5 patients without LRC 4 had a CMR and 1 a SMD. Out of 5 patients with distant metastases, 3 had a CMR and 2 a PMD. 1-year DFS and LRC were 80% and 90%, respectively

Radiomics signature learning (training set)

DFS

In univariate analysis, most clinical parameters and notably metabolic response (CMR vs. no CMR, $p=0.0001$) showed association with DFS without however reaching the corrected statistical significance, with HR between 2.3 and 4.3 (table 2). One texture from PET ($GLNU_{GLRLM-Q_E}$) and 4 from MRI (Inverse variance $_{GLCM-Q_F}$ and Entropy $_{GLCM-Q_F}$ in ADC maps from DWI, $RLVAR_{GLRLM-Q_L}$ in CE-MRI and $LZLGE_{GLSZM-Q_F}$ in T2) remained significant ($p<0.00001$), reaching HR between 5 and 34.

Only ADC Entropy $_{GLCM-Q_F}$ and CE-MRI $RLVAR_{GLRLM-Q_L}$ remained significantly correlated with DFS in multivariate analysis ($p<0.0001$ and $p=0.0001$ with hazard ratios of 31 and 11, respectively).

The estimated three-year DFS rates between patients with low versus high ADC Entropy $_{GLCM-Q_F}$ (cut-off 12.64) were 94% and 14%, respectively, and between patients with low versus high CE-MRI $RLVAR_{GLRLM-Q_L}$ (cut-off 0.17) 89% and 6%, respectively (figure 2).

LRC

One texture from PET/CT ($GLNU_{GLRLM-Q_E}$) and 3 from MRI (Inverse variance $_{GLCM-Q_F}$ and Entropy $_{GLCM-Q_F}$ in ADC map and $RLVAR_{GLRLM-Q_L}$ in CE-MRI) remained significantly correlated with LRC in univariate analysis after correction ($p<0.00001$, HR from 13 to 33), whereas none of the clinical factors reached statistical significance despite trends (p from 0.02 to 0.0007 and HR from 2 to 6) (table 3).

In multivariate analysis only ADC Entropy $_{GLCM-Q_F}$ ($p=0.0079$) and PET $GLNU_{GLRLM-Q_E}$ ($p=0.0043$) remained independent prognostic factors.

The estimated three-year LRC rates between patients with low versus high PET $GLNU_{GLRLM-Q_E}$ (cut-off 103.71) were 98% and 41%, and with low versus high ADC Entropy $_{GLCM-Q_F}$ (cut-off 12.64) were 98% and 45%. The combination of these 2 features provided an even better predictive model for LRC (98% vs. 18%) (figure 3).

Radiomics signature evaluation (testing set)

When applying the selected radiomics features with their optimal cut-off values determined in the training set to the testing set, we obtained promising performance.

ADC Entropy $_{GLCM-Q_F}$ (cut-off 12.64) reached an accuracy of 94% (sensitivity 90%, specificity 96%) to predict recurrence with a HR of 19.6 ($p<0.0001$), compared to 60% at best using standard factors (Figure 4).

For LRC, PET $GLNU_{GLRLM-Q_E}$ (cut-off 103.71) alone and its combination with ADC Entropy $_{GLCM-Q_F}$ reached accuracy of 94% (sensitivity 100%, specificity 93%) and 100% respectively (HRs undefined, $p=0.0001$ and $p<0.0001$), compared to 56% at best using standard factors (figure 5).

These features differentiate between patients with a high risk to develop distant metastasis and those with a high risk to develop an isolated locoregional relapse. A flowchart for personalized treatment management of these patients can be derived (figure 6).

DISCUSSION

Our results suggest that $GLNU_{GLRLM}$ in FDG PET and/or $Entropy_{GLCM}$ in ADC maps from DWI MRI are powerful predictors of the efficacy of CRT in the treatment of CC. Higher values of these parameters were associated with worse outcome, confirming that more heterogeneous tumors have a poor prognosis. These findings can be acted upon to tailor treatment (figure 6). Following this flowchart, more aggressive loco-regional treatment could be offered to patients with high-risk of an isolated loco-regional relapse whereas for patients with high-risk of distant relapse, a systemic adjuvant treatment would be more beneficial.

To our knowledge, this is the first study evaluating the prognostic value of radiomics exploiting both PET/CT and MRI images in LACC patients. Our results concur with previous studies in CC that exploited either PET or MRI. A first study associated high pretreatment PET $GLNU_{GLRLM}$ with poorer prognosis [9]. Another showed that ^{18}F -FDG PET/CT features could predict local recurrence of LACC better than SUV_{max} [13]. A third study showed that DCE-MRI 2nd-order textures could predict treatment outcome [10].

We showed PET/CT and MRI could provide complementary information when examinations are performed separately, as it is currently done in routine clinical practice. Similar investigations on hybrid imaging PET/MRI systems would be interesting because it would provide better temporal and spatial matching of the tumor volume in the different modalities, which could in addition facilitate its delineation. There is currently only a handful of radiomics studies using PET/MRI [25]. Given the small number of available PET/MRI systems, multi-centric investigations to validate radiomics models on these hybrid devices is also more challenging.

Our study has limitations. It was monocentric and retrospective, which is the case of most of radiomics studies [8], including in CC [9-13]. The number of patients was limited and we included a large number of parameters (more than 800), however we performed training and testing evaluation, and statistical significance was corrected for multiple testing in the univariate analysis, in order to avoid both false-discovery and overfitting. Before validating our radiomics signature on an external cohort (with different acquisition protocols), it was first necessary to validate it on patients from the same center. In that regard, the first 6 patients underwent PET/CT in a different scanner than the rest of the cohort. However in all cases the images were reconstructed with the same voxel size and the same post-reconstruction filter. The slice gap on T2-w and CE-MRI could impair 2nd- and 3rd-order features extraction. On ADC maps from DWI MRI however, there is no slice gap and this parameter was highlighted as one of the most efficient. In addition, all MRI pre-treatment were realized in the same center and with same acquisition and reconstruction protocols were used (supplemental material table 1) which limits the problems of reproducibility of radiomics features in MRI in particular as regards the geometric distortions. Finally, only primary tumors were characterized.

Beyond these potential sources of bias, radiomics is a promising approach but still suffers from inherent limitations which will need to be addressed before it can be used in clinical practice. Among these, the repeatability and robustness of the procedure has to be improved. Accurate segmentation is an important step of the feature extraction, as radiomics are derived from segmented volumes of interest. Manual delineation is a straightforward solution, but is very time consuming and suffers from high inter- and intra-observer variability [26]. Validated automatic or semi-automatic segmentation was used in our study to minimize manual input and increase consistency. The volumes derived from each image modality showed no significant differences (supplemental material figure 2C). In addition, the two features retained show low correlation with tumor volume and other clinical factors (supplemental material figure 1). 3D SlicerTM and the Growcut algorithm used are available for free and require minimal inputs from the user [27]. Although FLAB is not freely

available, other efficient PET segmentation tools are available in clinical stations, such as adaptive thresholding or gradient-based method [28], and our results should therefore be reproducible by others.

The choice of the optimal cut-off to stratify patients into a binary model can impact the results. This choice can be dependent on the training dataset and thus, hardly applicable to an external population. To confirm the predictive value of the features identified in a cohort, validation on an external cohort of patients is considered the gold standard [8, 29]. If this type of validation is not feasible, the best approach is to divide the available patients into training and testing sets, as we did. Validation of our findings is currently underway in a cohort of patients from a different clinical center.

Other factors such as image acquisition parameters [30], tumor volume [31], grey-level discretization and other pre-processing steps [8, 29] can influence radiomics findings. Acquisition parameters for both PET and MRI images were the same for all patients. One of the most important confounding factors in radiomics studies is the volume (i.e. the number of voxels). For PET radiomics specifically, textural features are unlikely to provide complementary information with respect to volume for the smallest lesions, due to the combination of the limited spatial resolution of PET imaging with the large voxel size sampling, leading to a small number of voxels to perform texture analysis. Although it has been suggested that a lower limit could be as high as 45 cm³ based on entropy_{GLCM} [ref Brooks], later studies have shown that this lower limit actually varies depending on the feature and the methodological choices for its calculation, such as the grey-levels discretization method or the texture matrices design, suggesting a lower limit around 5 to 10 cm³ instead, although this may not be applicable to all cases. Therefore it is rather recommended to include volume in the multivariate analysis, to report correlations and investigate the potential bias of the inclusion of the smallest volumes in the analysis [ref 29, 31]. In our study, the range of considered volumes was 5-97 cm³ with rather large mean and median values of 33 and 27 cm³ respectively, which corresponds to 625 voxels for the smallest volume but a mean and median number of 4171 and 3381 voxels respectively. In addition, GLNU_{GLRLM-Q_E} showed limited correlation with PET volume and had similar value in both training and testing sets for tumors below or above thresholds of 45 or 20 cm³ (supplemental table 3 and supplemental figures 3 and 4). Although tumor volume or intensity-based measurements from both PET and MRI sequences were correlated with the endpoints they had insufficient predictive power compared to higher order radiomics features to be retained in the univariate analysis. In addition, the levels of correlation the retained features exhibit with volume or other confounding factors demonstrate they are not merely surrogates of usual variables (see supplemental material). This shows that the radiomics features we identified provide complementary information with respect to volume in both PET and MRI and that there is no bias in our results coming from the inclusion of the smallest lesions.

In most studies, the number of features is often far greater than the number of patients included, potentially leading to a high risk of false positive-rate, as recently highlighted [8, 22, 29]. There is no consensus about the unsupervised approach to obtain the best results. A recent study investigated a large panel of machine-learning approaches for radiomics-based survival prediction, considering both features selection and classification methods [32]. Their variability analysis pointed out that the choice of the classification method has the highest impact on performance variation in predicting the OS (more than 30% of the total variation), with respect to the choice of features selection method (only 6% of variation). In our study we could obtain near-perfect accuracy by using only the one or two parameters that remained significant after correction for multiple testing, and the use of advanced machine learning was thus deemed not necessary.

We identified features with high predictive power regarding tissue response to radiation, however the biological interpretation of these features remains an area of active investigations [33, 34]. As

first elements of interpretation, PET $GLNU_{GLRLM-Q_E}$ and ADC Entropy $_{GLCM-Q_F}$ are both computed on functional imaging. Entropy $_{GLCM-Q_F}$ calculated on the ADC map derived from DWI MRI could be linked to a cellularity heterogeneity and expression of growth factor. PET $GLNU_{GLRLM-Q_E}$ might be associated to a necrosis heterogeneity and expression of vascular growth factor. More comprehensive assessment of the molecular features of patients based on tumor specimen characterization and noninvasive molecular imaging approaches are required to further investigate these hypotheses [33, 34].

CONCLUSIONS

Radiomics features such as $GLNU_{GLRLM}$ on ^{18}F -FDG PET and Entropy $_{GLCM}$ on ADC maps derived from DW-MRI were independent prognostic factors for disease outcome in LACC patients undergoing CRT, with significantly higher value than conventional factors. The identification of high-risk patients at diagnosis can allow tailored treatments involving higher doses of radiation boost, consolidation chemotherapy, and/or adjuvant hysterectomy, when indicated, and should be confirmed in external cohorts and prospective studies. The biological interpretation of radiomics remains an open question warranting further investigation.

Compliance with Ethical Standards:

Conflict of Interest: Author François Lucia declares that he has no conflict of interest. Author Dimitris Visvikis declares that he has no conflict of interest. Author Marie-Charlotte Desseroit declares that she has no conflict of interest. Author Omar Miranda declares that he has no conflict of interest. Author Jean-Pierre Malhaire declares that he has no conflict of interest. Author Philippe Robin declares that he has no conflict of interest. Author Olivier Pradier declares that he has no conflict of interest. Author Mathieu Hatt declares that he has no conflict of interest. Author Ulrike Schick declares that she has no conflict of interest.

Ethical approval: All procedures performed in studies involving human participants were in accordance with the ethical standards of the institutional and/or national research committee and with the 1964 Helsinki declaration and its later amendments or comparable ethical standards.

Informed consent: Informed consent was obtained from all individual participants included in the study.

REFERENCES

1. Ferlay J, Soerjomataram I, Dikshit R, Eser S, Mathers C, Rebelo M, Parkin DM, Forman D, Bray F: **Cancer incidence and mortality worldwide: sources, methods and major patterns in GLOBOCAN 2012.** *International journal of cancer* 2015, **136**(5):E359-386.
2. Rose PG, Java J, Whitney CW, Stehman FB, Lanciano R, Thomas GM, DiSilvestro PA: **Nomograms Predicting Progression-Free Survival, Overall Survival, and Pelvic Recurrence in Locally Advanced Cervical Cancer Developed From an Analysis of Identifiable Prognostic Factors in Patients From NRG Oncology/Gynecologic Oncology Group Randomized Trials of Chemoradiotherapy.** *Journal of clinical oncology : official journal of the American Society of Clinical Oncology* 2015, **33**(19):2136-2142.
3. Moore KN, Java JJ, Slaughter KN, Rose PG, Lanciano R, DiSilvestro PA, Thigpen JT, Lee YC, Tewari KS, Chino J *et al*: **Is age a prognostic biomarker for survival among women with locally advanced cervical cancer treated with chemoradiation? An NRG Oncology/Gynecologic Oncology Group ancillary data analysis.** *Gynecologic oncology* 2016, **143**(2):294-301.
4. Herrera FG, Prior JO: **The role of PET/CT in cervical cancer.** *Frontiers in oncology* 2013, **3**:34.
5. Choi J, Kim HJ, Jeong YH, Lee JH, Cho A, Yun M, Lee JD, Kim YB, Kim YT, Kang WJ: **The Role of (18) F-FDG PET/CT in Assessing Therapy Response in Cervix Cancer after Concurrent Chemoradiation Therapy.** *Nuclear medicine and molecular imaging* 2014, **48**(2):130-136.
6. Lambin P, Rios-Velazquez E, Leijenaar R, Carvalho S, van Stiphout RG, Granton P, Zegers CM, Gillies R, Boellard R, Dekker A *et al*: **Radiomics: extracting more information from medical images using advanced feature analysis.** *European journal of cancer* 2012, **48**(4):441-446.
7. Rios Velazquez E, Parmar C, Liu Y, Coroller TP, Cruz G, Stringfield O, Ye Z, Makrigiorgos M, Fennessy F, Mak RH *et al*: **Somatic Mutations Drive Distinct Imaging Phenotypes in Lung Cancer.** *Cancer research* 2017, **77**(14):3922-3930.
8. Yip SS, Aerts HJ: **Applications and limitations of radiomics.** *Physics in medicine and biology* 2016, **61**(13):R150-166.
9. Ho KC, Fang YH, Chung HW, Yen TC, Ho TY, Chou HH, Hong JH, Huang YT, Wang CC, Lai CH: **A preliminary investigation into textural features of intratumoral metabolic heterogeneity in (18)F-FDG PET for overall survival prognosis in patients with bulky cervical cancer treated with definitive concurrent chemoradiotherapy.** *American journal of nuclear medicine and molecular imaging* 2016, **6**(3):166-175.
10. Torheim T, Groendahl AR, Andersen EK, Lyng H, Malinen E, Kvaal K, Futsaether CM: **Cluster analysis of dynamic contrast enhanced MRI reveals tumor subregions related to locoregional relapse for cervical cancer patients.** *Acta oncologica* 2016, **55**(11):1294-1298.
11. Chung HH, Kang SY, Ha S, Kim JW, Park NH, Song YS, Cheon GJ: **Prognostic value of preoperative intratumoral FDG uptake heterogeneity in early stage uterine cervical cancer.** *J Gynecol Oncol* 2016, **27**(2):e15.
12. Guan Y, Li W, Jiang Z, Chen Y, Liu S, He J, Zhou Z, Ge Y: **Whole-Lesion Apparent Diffusion Coefficient-Based Entropy-Related Parameters for Characterizing Cervical Cancers: Initial Findings.** *Acad Radiol* 2016, **23**(12):1559-1567.
13. Reuze S, Orhac F, Chargari C, Nioche C, Limkin E, Riet F, Escande A, Haie-Meder C, Derclé L, Gouy S *et al*: **Prediction of cervical cancer recurrence using textural features extracted from 18F-FDG PET images acquired with different scanners.** *Oncotarget* 2017, **8**(26):43169-43179.
14. https://www.nccn.org/professionals/physician_gls/pdf/cervical.pdf.
15. Lim K, Small W, Jr., Portelance L, Creutzberg C, Jurgenliemk-Schulz IM, Mundt A, Mell LK, Mayr N, Viswanathan A, Jhingran A *et al*: **Consensus guidelines for delineation of clinical target volume for intensity-modulated pelvic radiotherapy for the definitive treatment of**

- cervix cancer**. *International journal of radiation oncology, biology, physics* 2011, **79**(2):348-355.
16. Wahl RL, Jacene H, Kasamon Y, Lodge MA: **From RECIST to PERCIST: Evolving Considerations for PET response criteria in solid tumors**. *Journal of nuclear medicine : official publication, Society of Nuclear Medicine* 2009, **50** Suppl 1:122S-150S.
 17. Hatt M, Cheze le Rest C, Turzo A, Roux C, Visvikis D: **A fuzzy locally adaptive Bayesian segmentation approach for volume determination in PET**. *IEEE transactions on medical imaging* 2009, **28**(6):881-893.
 18. Hatt M, Cheze le Rest C, Descourt P, Dekker A, De Ruyscher D, Oellers M, Lambin P, Pradier O, Visvikis D: **Accurate automatic delineation of heterogeneous functional volumes in positron emission tomography for oncology applications**. *International journal of radiation oncology, biology, physics* 2010, **77**(1):301-308.
 19. Velazquez ER, Parmar C, Jermoumi M, Mak RH, van Baardwijk A, Fennessy FM, Lewis JH, De Ruyscher D, Kikinis R, Lambin P *et al*: **Volumetric CT-based segmentation of NSCLC using 3D-Slicer**. *Scientific reports* 2013, **3**:3529.
 20. Alex Zwanenburg SL, Martin Vallières, Steffen Löck: **Image biomarker standardisation initiative - feature definitions**. 2017.
 21. Desseroit MC, et al: **Comparison of three quantization methods for the calculation of textural features in PET/CT images: impact on prognostic models in Non-Small Cell Lung Cancer**. *IEEE Nuclear Science Symposium and Medical Imaging Conference 2016* 2016.
 22. Chalkidou A, O'Doherty MJ, Marsden PK: **False Discovery Rates in PET and CT Studies with Texture Features: A Systematic Review**. *PloS one* 2015, **10**(5):e0124165.
 23. Collins GS, Reitsma JB, Altman DG, Moons KG: **Transparent reporting of a multivariable prediction model for individual prognosis or diagnosis (TRIPOD): the TRIPOD Statement**. *European journal of clinical investigation* 2015, **45**(2):204-214.
 24. Naik A, Gurjar OP, Gupta KL, Singh K, Nag P, Bhandari V: **Comparison of dosimetric parameters and acute toxicity of intensity-modulated and three-dimensional radiotherapy in patients with cervix carcinoma: A randomized prospective study**. *Cancer radiotherapie : journal de la Societe francaise de radiotherapie oncologique* 2016, **20**(5):370-376.
 25. Antunes J, Viswanath S, Rusu M, Valls L, Hoimes C, Avril N, Madabhushi A: **Radiomics Analysis on FLT-PET/MRI for Characterization of Early Treatment Response in Renal Cell Carcinoma: A Proof-of-Concept Study**. *Translational oncology* 2016, **9**(2):155-162.
 26. Eminowicz G, McCormack M: **Variability of clinical target volume delineation for definitive radiotherapy in cervix cancer**. *Radiotherapy and oncology : journal of the European Society for Therapeutic Radiology and Oncology* 2015, **117**(3):542-547.
 27. Egger J, Kapur T, Fedorov A, Pieper S, Miller JV, Veeraraghavan H, Freisleben B, Golby AJ, Nimsy C, Kikinis R: **GBM volumetry using the 3D Slicer medical image computing platform**. *Scientific reports* 2013, **3**:1364.
 28. Hatt M, Lee JA, Schmidtlein CR, Naqa IE, Caldwell C, De Bernardi E, Lu W, Das S, Geets X, Gregoire V *et al*: **Classification and evaluation strategies of auto-segmentation approaches for PET: Report of AAPM task group No. 211**. *Medical physics* 2017, **44**(6):e1-e42.
 29. Hatt M, Tixier F, Pierce L, Kinahan PE, Le Rest CC, Visvikis D: **Characterization of PET/CT images using texture analysis: the past, the present... any future?** *European journal of nuclear medicine and molecular imaging* 2017, **44**(1):151-165.
 30. Galavis PE, Hollensen C, Jallow N, Paliwal B, Jeraj R: **Variability of textural features in FDG PET images due to different acquisition modes and reconstruction parameters**. *Acta oncologica* 2010, **49**(7):1012-1016.
 31. Hatt M, Majdoub M, Vallieres M, Tixier F, Le Rest CC, Groheux D, Hindie E, Martineau A, Pradier O, Hustinx R *et al*: **18F-FDG PET uptake characterization through texture analysis: investigating the complementary nature of heterogeneity and functional tumor volume in a multi-cancer site patient cohort**. *Journal of nuclear medicine : official publication, Society of Nuclear Medicine* 2015, **56**(1):38-44.

32. Parmar C, Grossmann P, Bussink J, Lambin P, Aerts HJ: **Machine Learning methods for Quantitative Radiomic Biomarkers**. *Scientific reports* 2015, **5**:13087.
33. Incoronato M, Aiello M, Infante T, Cavaliere C, Grimaldi AM, Mirabelli P, Monti S, Salvatore M: **Radiogenomic Analysis of Oncological Data: A Technical Survey**. *International journal of molecular sciences* 2017, **18**(4).
34. Cancer Genome Atlas Research N, Albert Einstein College of M, Analytical Biological S, Barretos Cancer H, Baylor College of M, Beckman Research Institute of City of H, Buck Institute for Research on A, Canada's Michael Smith Genome Sciences C, Harvard Medical S, Helen FGCC *et al*: **Integrated genomic and molecular characterization of cervical cancer**. *Nature* 2017, **543**(7645):378-384.

Table 1: Patients' characteristics

	Training set		Testing set		Difference (p-value)
	n=69	%	n=33	%	
Age median (range)	58 (29-90)		57 (37-86)		0.96
FIGO stage					
IB1	2	3	1	3	0.85
IB2	8	12	4	12	
IIA	4	6	3	9	
IIB	36	52	15	46	
IIIA	1	1	1	3	
IIIB	9	13	5	15	
IVA	9	13	4	12	
Histology					
Squamous	54	79	26	79	0.83
Adenocarcinoma	9	13	5	15	
Adenosquamous carcinoma	1	1	0	0	
Clear cell carcinoma	5	7	2	6	
Lymph node involvement					
Uninvolved	30	44	20	61	0.21
Involved	39	56	13	39	
pelvic	27	69	8	62	
pelvic and para-aortic	12	31	5	38	
CBC median (range)					
white blood cells	8.3 · 10 ³ /mL (4.6-25.6)		7.6 · 10 ³ /mL (5.1-20.6)		0.32
hemoglobin	128 g/dL (71-149)		126 g/dL (80-151)		0.91
platelets	261.5 · 10 ³ /mL (186-819)		227.3 · 10 ³ /mL (171-603)		0.27
body-mass index median (range)	23.2 (14-42)		22.6 (16-35)		0.61
Treatment					
3D-CRT	59	86	7	21	<0.0001
IMRT	10	14	26	79	
EBRT dose median (range)	45 (45-54)		45 (45-54)		0.52
BT dose median (range)	24 (21-26)		24 (21-28)		0.63
Overall treatment time (range)	49 (47-52)		49 (48-53)		0.47

Abbreviations: FIGO= International Federation of Gynecology and Obstetrics, CBC= complete blood counts, 3D-CRT= three-dimensional conformal radiotherapy, IMRT= intensity-modulated photon radiotherapy, EBRT= external beam radiotherapy, BT=brachytherapy

Table 2: Univariate and multivariate analysis for disease-free survival

Variables	Univariate analysis			Multivariate analysis		
	HR	95% CI	p	HR	95% CI	p
Histology (SCC vs. no SCC)	2.34	0.82-6.68	0.04	-	-	-
FIGO stage (I-II vs. III-IV)	3.33	1.29-8.62	0.0014	-	-	-
Tumor size (≤ 4.8 cm vs. > 4.8 cm)	2.83	1.29-6.21	0.014	-	-	-
Nodal stage (N1 vs. N0)	3.21	1.47-7.04	0.0081	-	-	-
Post-treatment metabolic response (CMR vs. no CMR)	4.31	1.82-10.26	0.0001	-	-	-
Volume PET (≤ 30 cc vs. > 30 cc)	2.09	0.94-4.62	0.06	-	-	-
Volume DWI-MRI (≤ 31 cc vs. > 31 cc)	2.38	0.97-4.91	0.06	-	-	-
SUV _{min} (≤ 5.9 vs. > 5.9)	0.8	0.53-1.64	0.16	-	-	-
SUV _{max} (≤ 23 vs. > 23)	0.53	0.23-1.24	0.2	-	-	-
ADC _{min} (≤ 91 vs. > 91)	1.73	0.71-3.67	0.1	-	-	-
ADC _{max} (≤ 2389 vs. > 2389)	1.89	0.79-3.81	0.09	-	-	-
ADC Entropy _{GLCM-Q_F}	34.18	13.85-84.34	<0.00001	30.95	7.01-136.59	<0.00001
CE-MRI RLVAR _{GLRLM-Q_L}	16.64	5.95-46.53	<0.00001	11.33	3.29-39.03	0.0001
PET GLNU _{GLRLM-Q_E}	5.39	2.33-12.47	<0.00001	-	-	-
T2 LZLGE _{GLSZM-Q_F}	5.08	2.11-11.93	<0.00001	-	-	-
ADC Inverse variance _{GLCM-Q_F}	5.03	2.05-11.78	<0.00001	-	-	-

Table 3: Univariate and multivariate analysis for loco-regional control

Variables	Univariate analysis			Multivariate analysis		
	HR	95% CI	p	HR	95% CI	p
Histology (SCC vs. non SCC)	2.48	0.64-9.61	0.09	-	-	-
FIGO stage (I-II vs. III-IV)	3.27	0.95-11.28	0.019	-	-	-
Tumor size (≤ 4.8 cm vs. > 4.8 cm)	4.73	1.57-14.21	0.0037	-	-	-
Nodal stage (N1 vs. N0)	3.35	1.17-9.55	0.048	-	-	-
Post-treatment metabolic response (CMR vs. no CMR)	5.87	1.87-18.45	0.0007	-	-	-
Volume PET (≤ 30 cc vs. > 30 cc)	2.49	0.66-9.63	0.08	-	-	-
Volume DWI-MRI (≤ 31 cc vs. > 31 cc)	2.59	0.73-9.81	0.06	-	-	-
SUV _{min} (≤ 5.9 vs. > 5.9)	1.21	0.49-7.13	0.22	-	-	-
SUV _{max} (≤ 23 vs. > 23)	1.04	0.37-6.85	0.29	-	-	-
ADC _{min} (≤ 91 vs. > 91)	2.26	0.51-9.46	0.11	-	-	-
ADC _{max} (≤ 2389 vs. > 2389)	2.38	0.57-9.55	0.1	-	-	-
ADC Entropy _{GLCM-Q_F}	28.10	9.11-86.66	<0.00001	16.35	2.10-126.94	0.0079
CE-MRI RLVAR _{GLRLM-Q_L}	13.22	3.71-47.11	<0.00001	-	-	-
PET GLNU _{GLRLM-Q_E}	33.11	10.34-106.06	<0.00001	20.01	2.59-154.89	0.0043
ADC Inverse variance _{GLCM-Q_F}	11.53	3.50-44.84	<0.00001	-	-	-

Abbreviations: FIGO=International Federation of Gynecology and Obstetrics, SCC= Squamous cell carcinoma, CMR=Complete metabolic response, GLCM=Grey-level Co-occurrence Matrix, GLRLM= Grey-level Run-Length matrix, GLSZM= Grey-level Size Zone matrix, RLVAR=Run Length Variance, GLNU=Grey-level non-uniformity, LZLGE= Large Zone Low Grey-Level Emphasis, vs= versus, HR=Hazard ratio, CI=Confidence Interval, MRI= magnetic resonance imaging, CE-MRI=contrast enhancement magnetic resonance imaging, PET= positron emission tomography , ADC=Apparent Diffusion Coefficient

Figure 1: Workflow

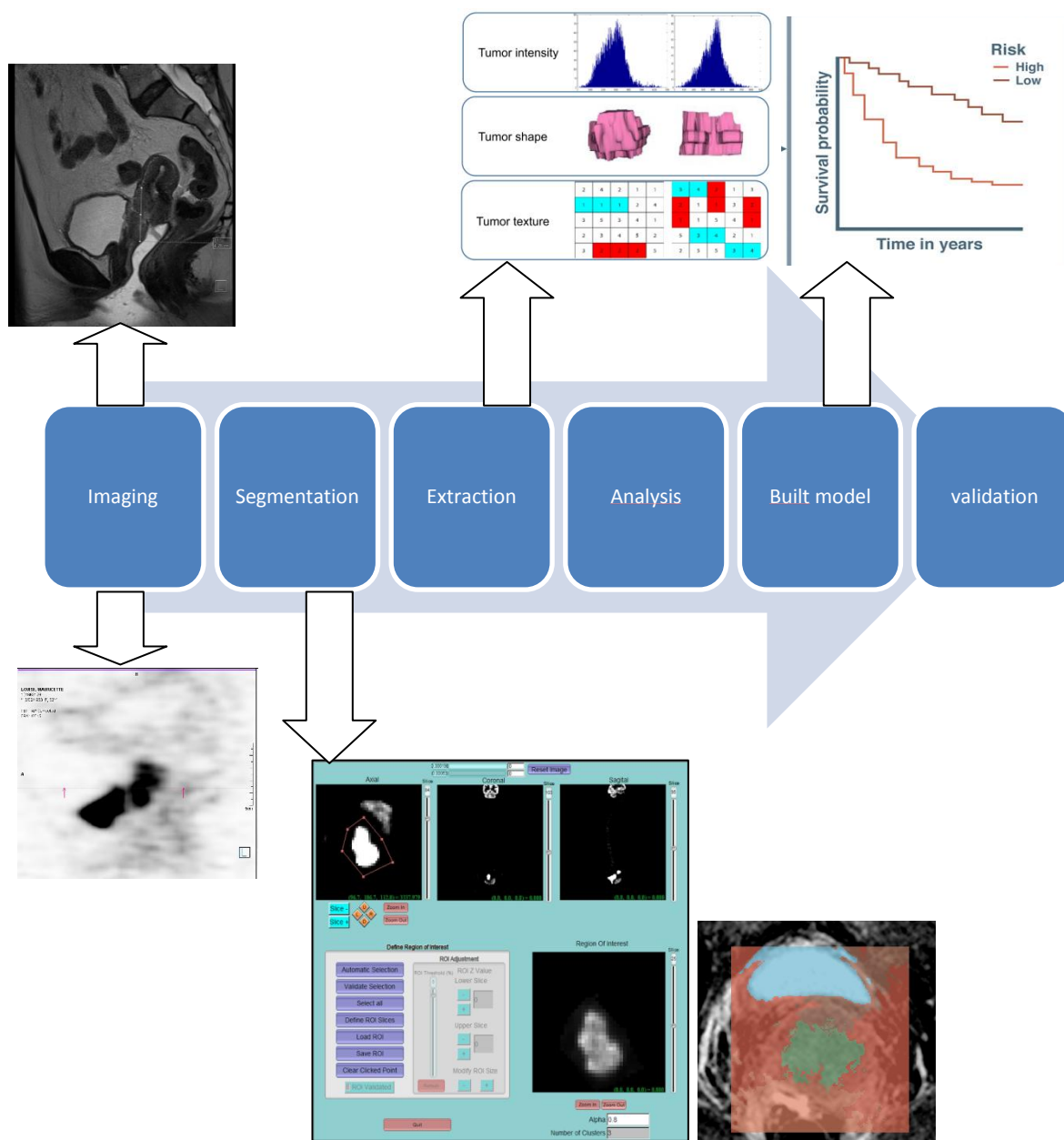
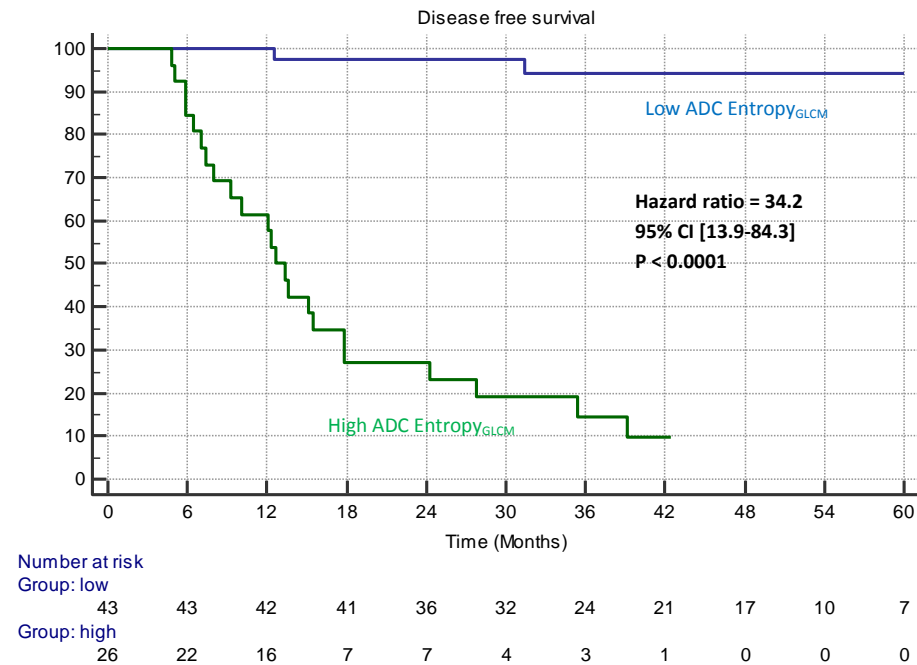
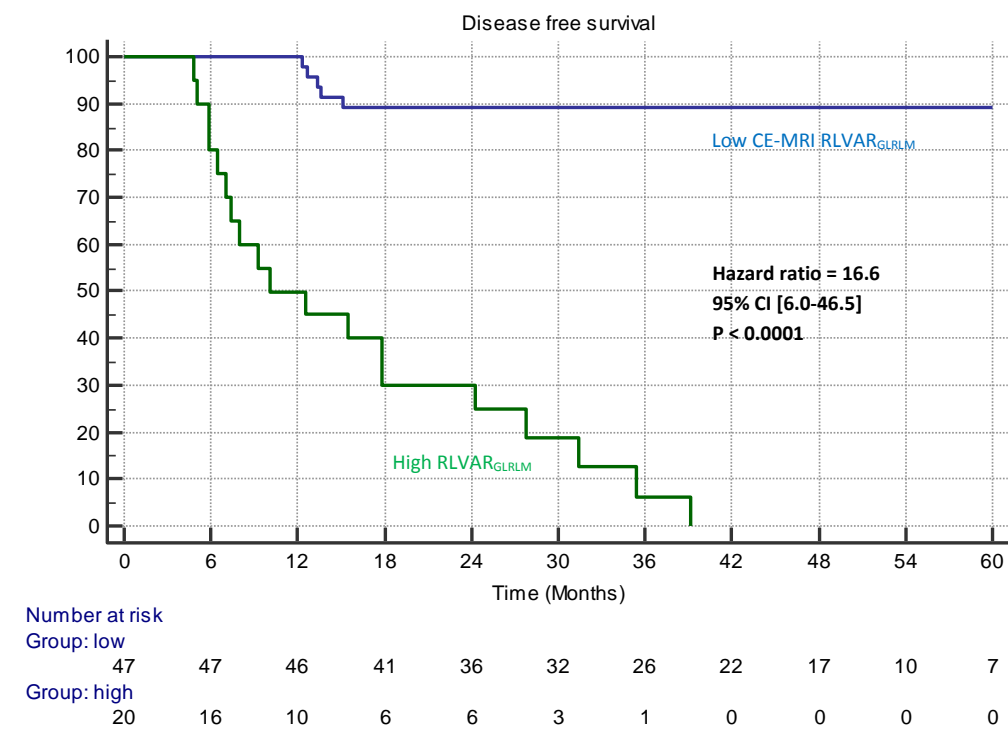


Figure 2: Kaplan-Meier estimates of disease-free survival (training set) according to (A) ADC Entropy_{G_{LCM}}, (B) CE-MRI RLVAR_{GLRLM}, (C) FIGO stage, (D) tumor size, (E) N stage and (F) metabolic response from PET/CT (assessed 2 to 3 months after treatment completion). (G) Comparison of ROC curves for ADC Entropy_{G_{LCM}} in comparison with clinico-pathological features.

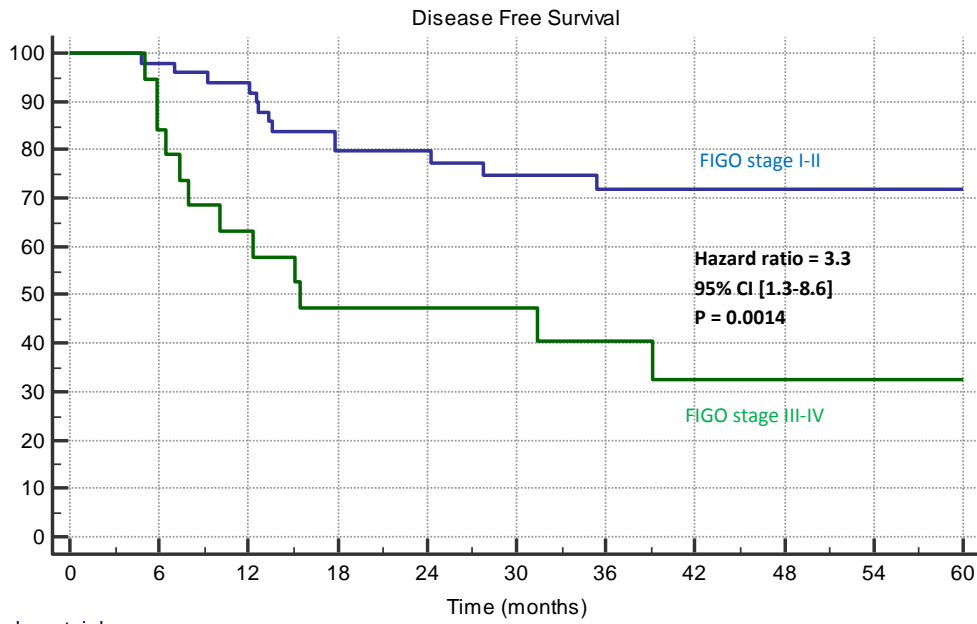
A



B



C



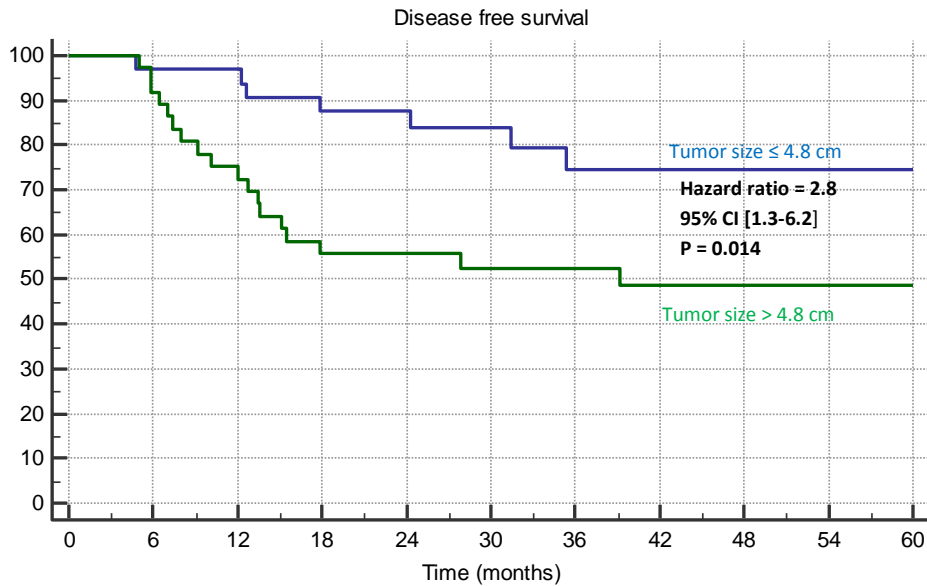
Number at risk
Group: 0

50	49	46	39	35	29	23	21	17	9	6
----	----	----	----	----	----	----	----	----	---	---

Group: 1

19	16	12	9	8	7	5	1	1	1	1
----	----	----	---	---	---	---	---	---	---	---

D



Number at risk

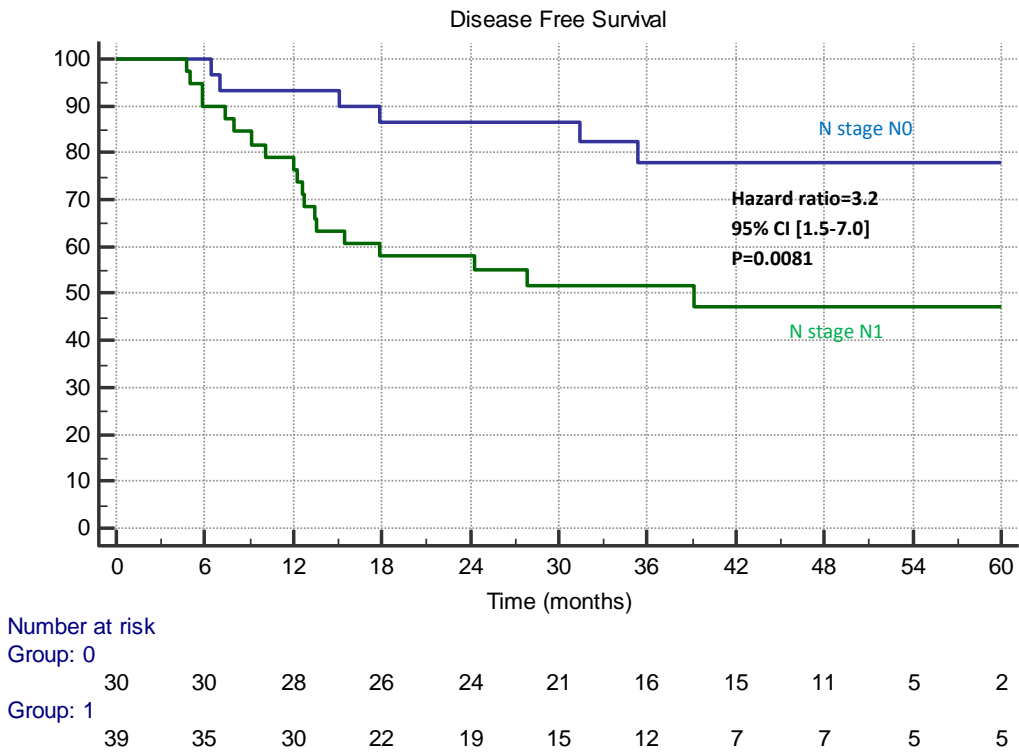
Group: 0

32	31	31	28	25	21	14	12	11	5	4
----	----	----	----	----	----	----	----	----	---	---

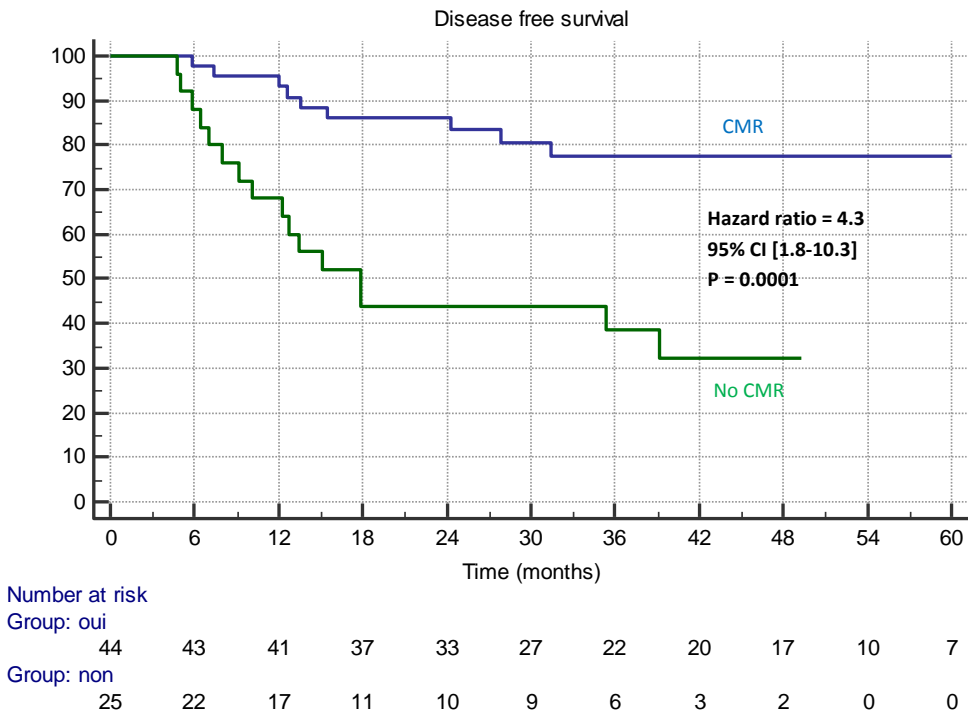
Group: 1

37	34	27	20	18	15	14	11	8	5	3
----	----	----	----	----	----	----	----	---	---	---

E



F



G

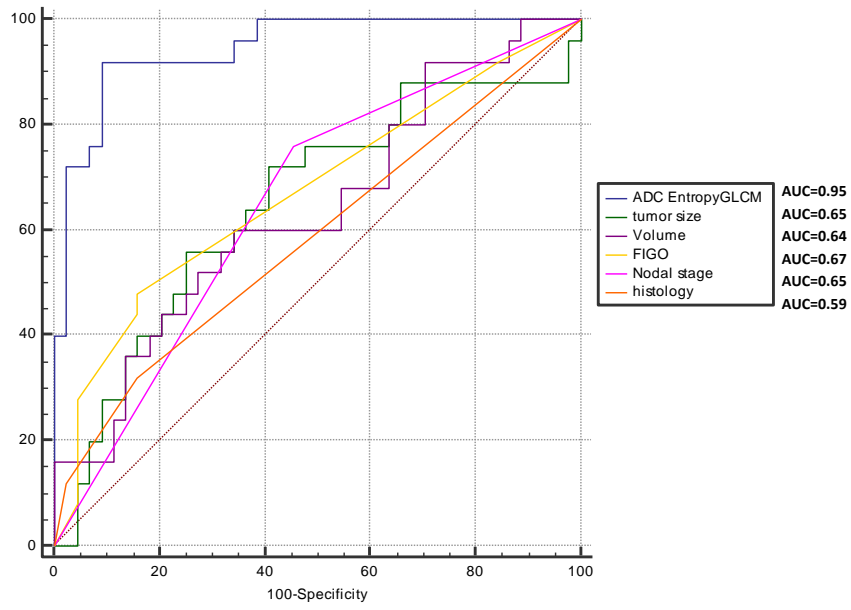
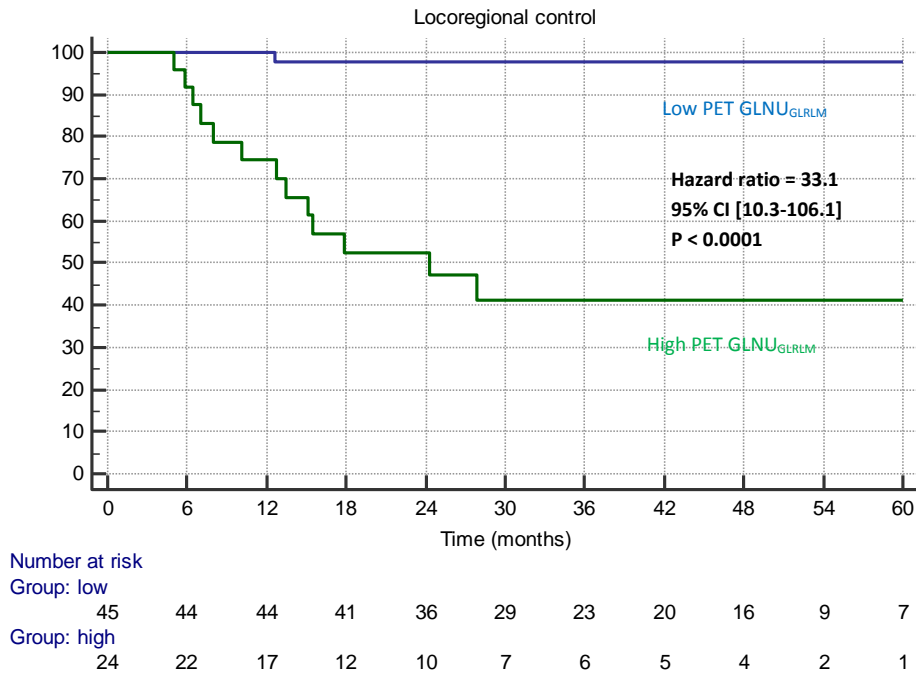
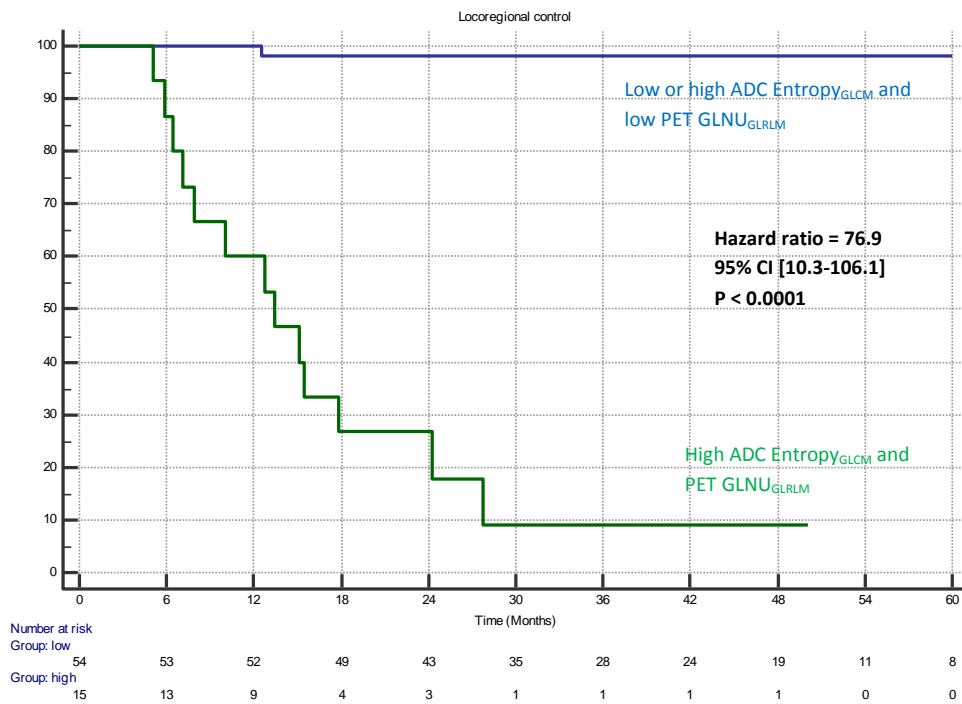


Figure 3: Kaplan-Meier estimates of locoregional control (training set) according to (A) PET GLNU_{GLRLM}, (B) the combination of ADC Entropy_{GLCM} and PET GLNU_{GLRLM}, (C) FIGO stage, (D) tumor size, (E) N stage and (F) metabolic response from PET/CT (assessed 2 to 3 months after treatment completion). (G) Comparison of ROC curves for PET GLNU_{GLRLM} in comparison with clinico-pathological features.

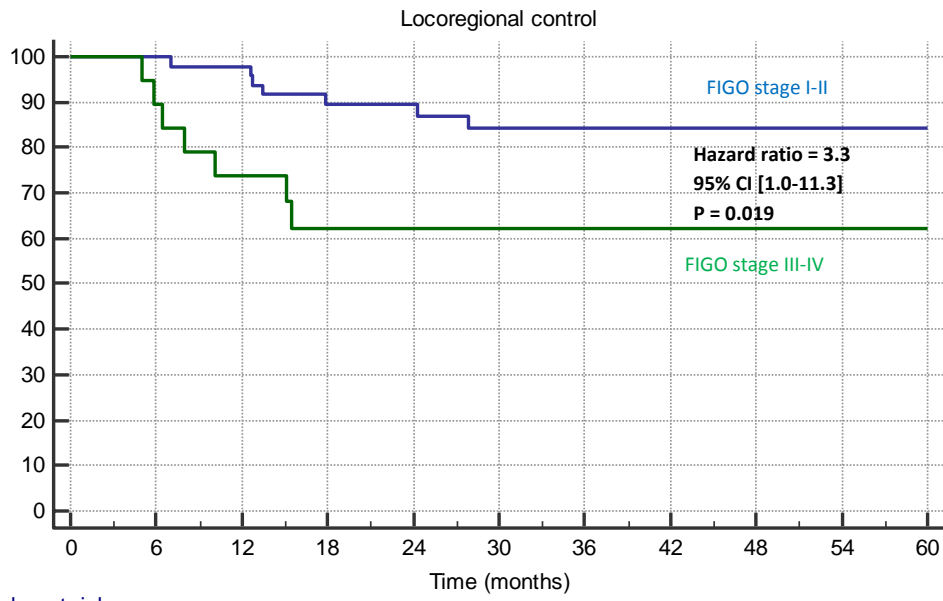
A



B



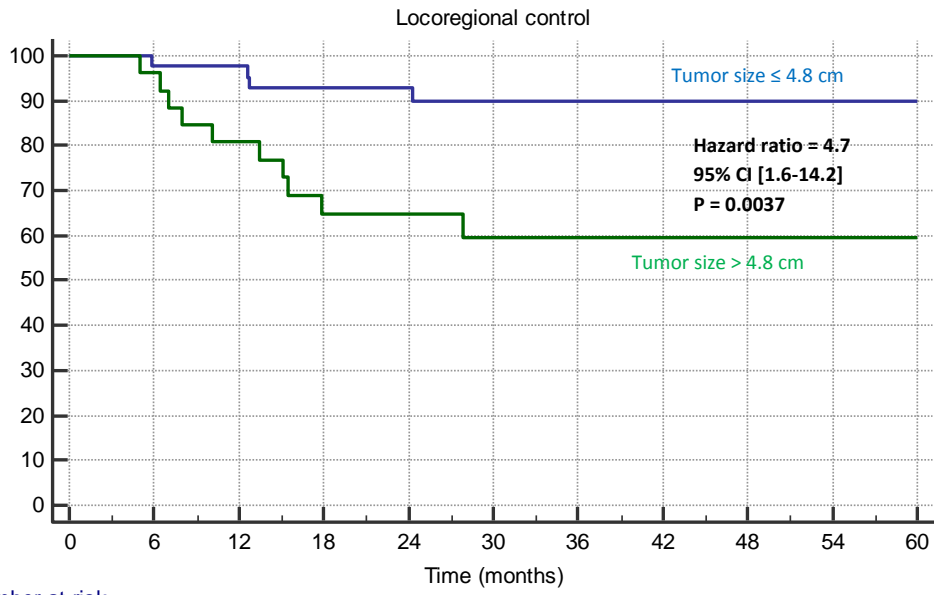
C



Number at risk

Time (months)	0	6	12	18	24	30	36	42	48	54	60
Group: 0	50	49	47	42	37	31	24	23	19	9	6
Group: 1	19	17	14	11	9	7	6	3	3	2	2

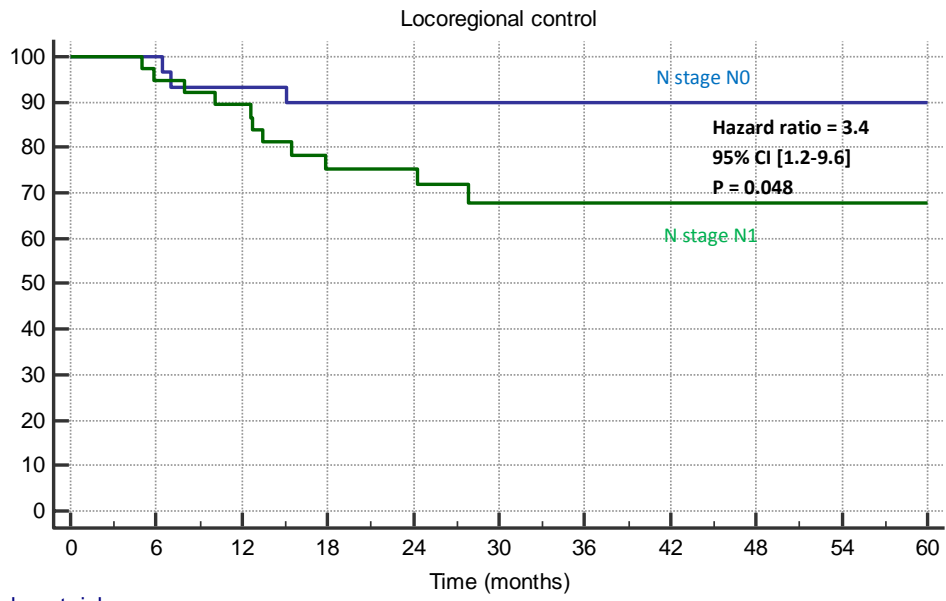
D



Number at risk

Time (months)	0	6	12	18	24	30	36	42	48	54	60
Group: 0	43	41	40	37	33	28	21	18	17	9	7
Group: 1	26	25	21	16	13	10	9	8	5	2	1

E



Number at risk

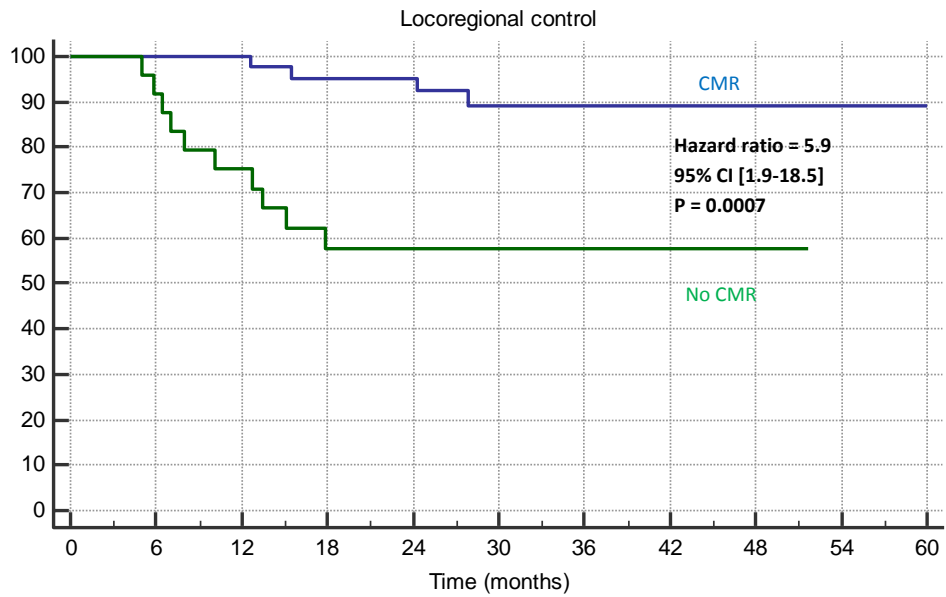
Group: 0

30 30 28 27 25 22 18 17 14 6 3

Group: 1

39 36 33 26 21 16 12 9 8 5 5

F



Number at risk

Group: 1

44 44 43 40 34 28 23 21 18 11 8

Group: 2

25 22 18 13 12 10 7 5 4 0 0

G

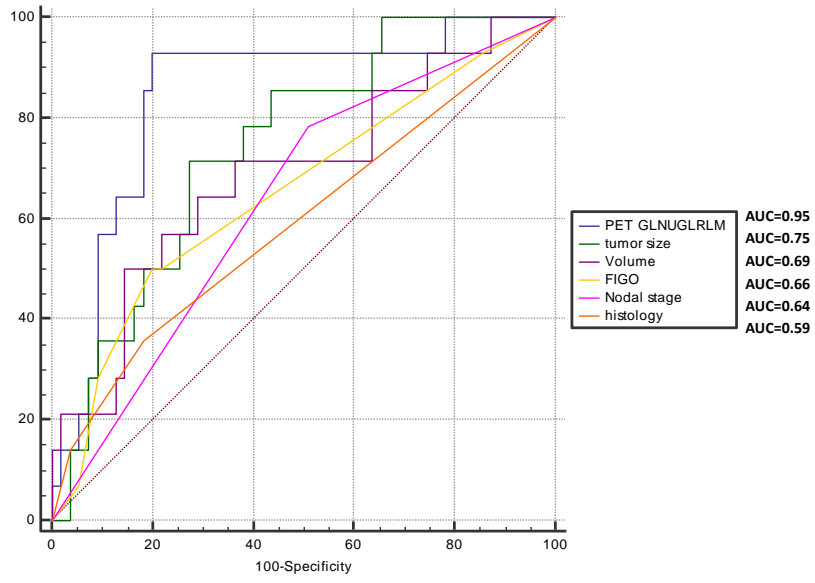
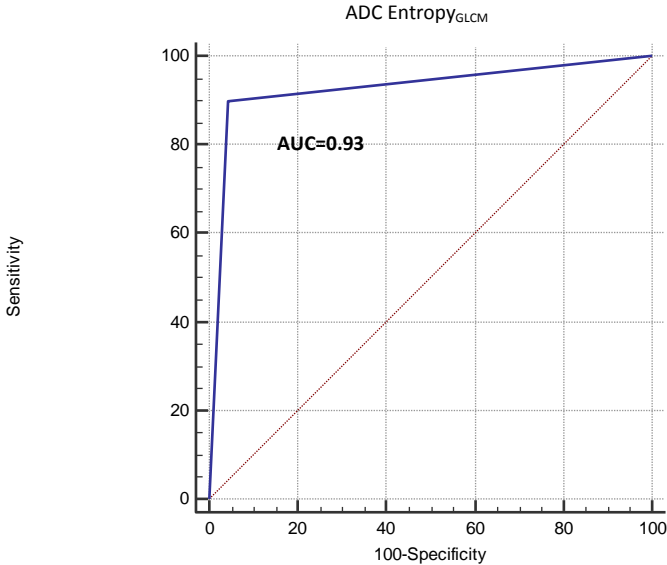
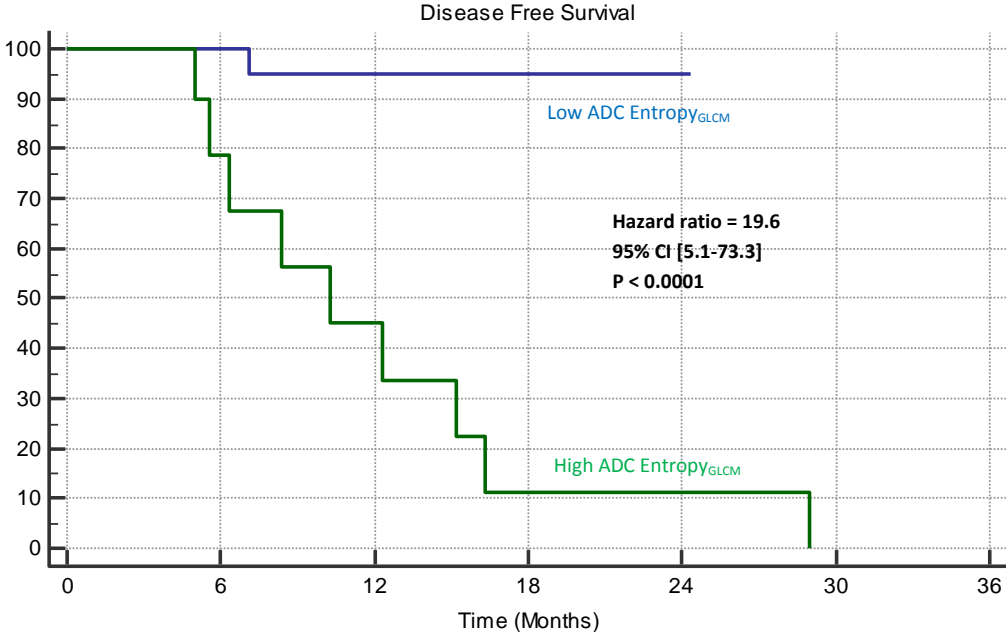


Figure 4: Prediction of disease-free survival in the testing set according to ADC Entropy_{GLCM} with (A) ROC curve and (B) resulting Kaplan-Meier curve.

A



B

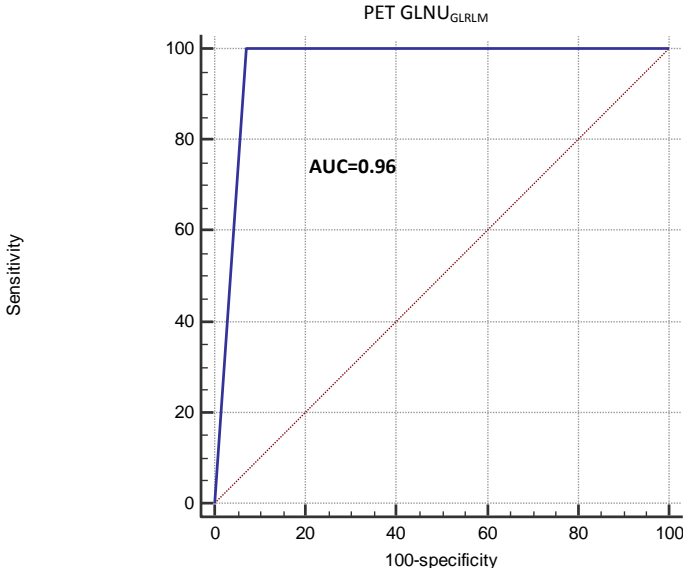


Number at risk

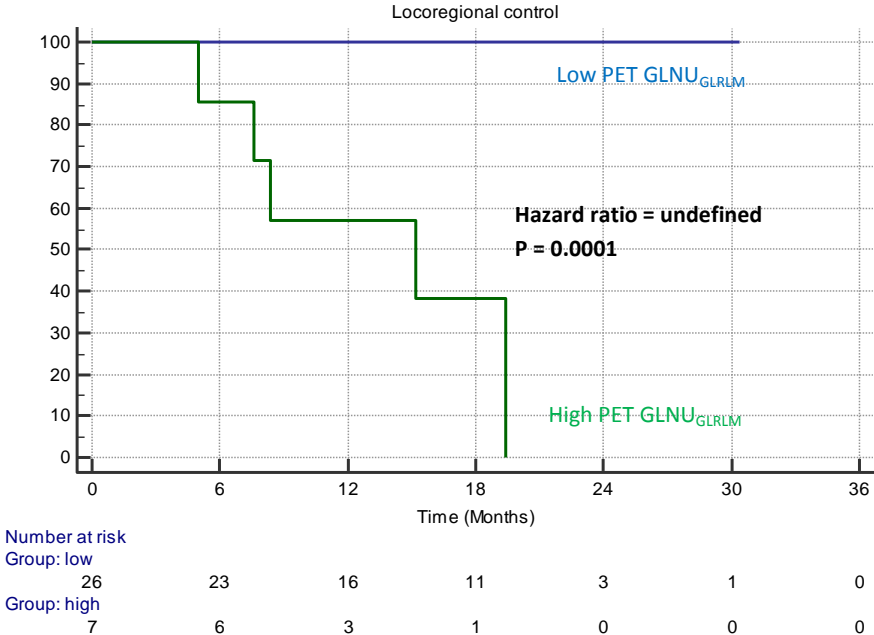
Group: low	23	21	13	8	2	0
Group: high	10	7	4	1	1	0

Figure 5: Prediction of locoregional control in the testing set according to (A-B) PET GLNU_{GLRLM} alone or to (C-D) its combination with ADC Entropy_{GLCM} with (A, C) ROC curves and (C, D) the resulting Kaplan-Meier curves.

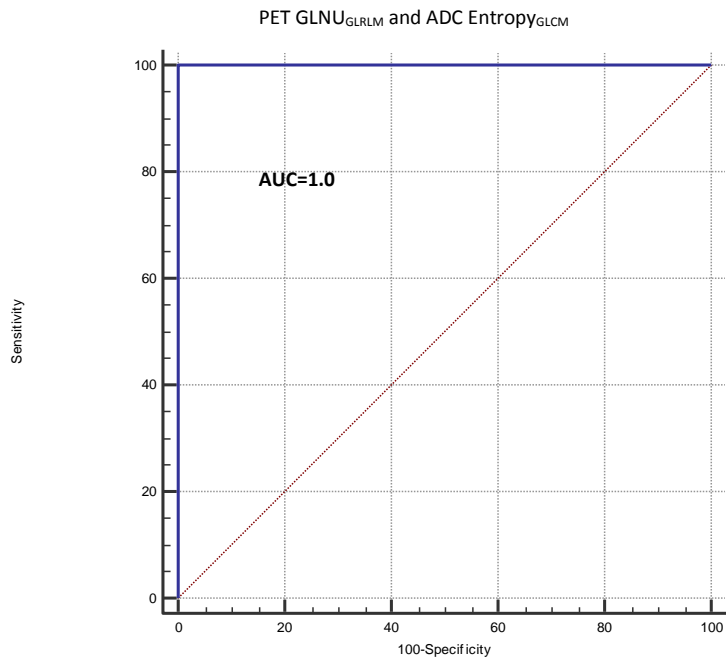
A



B



C



D

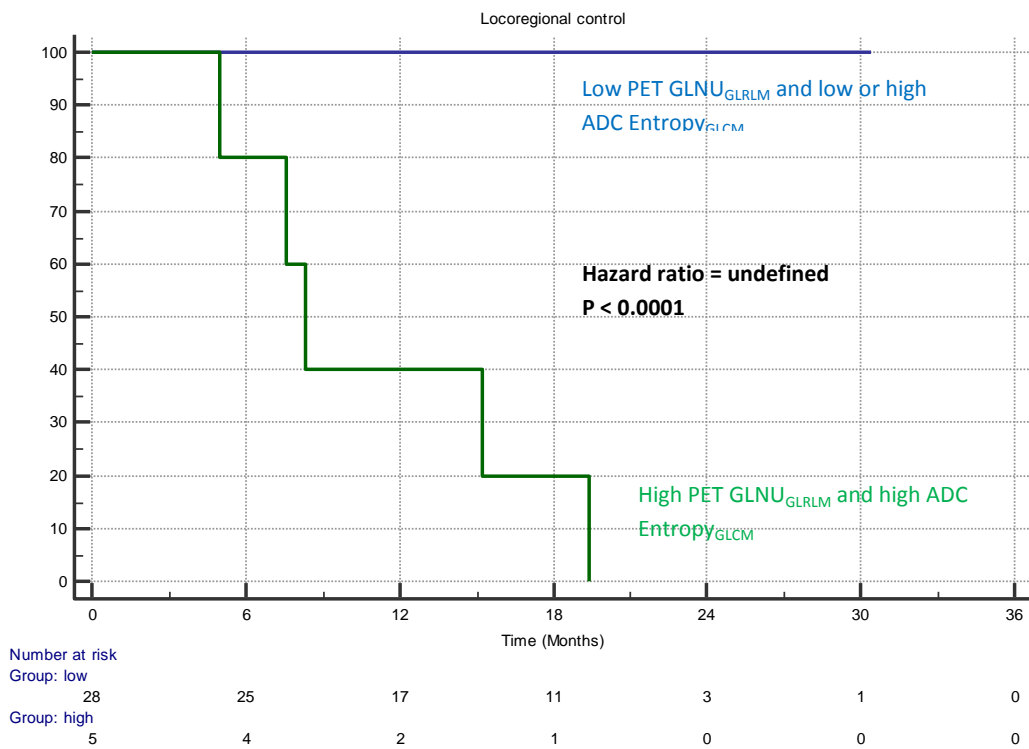
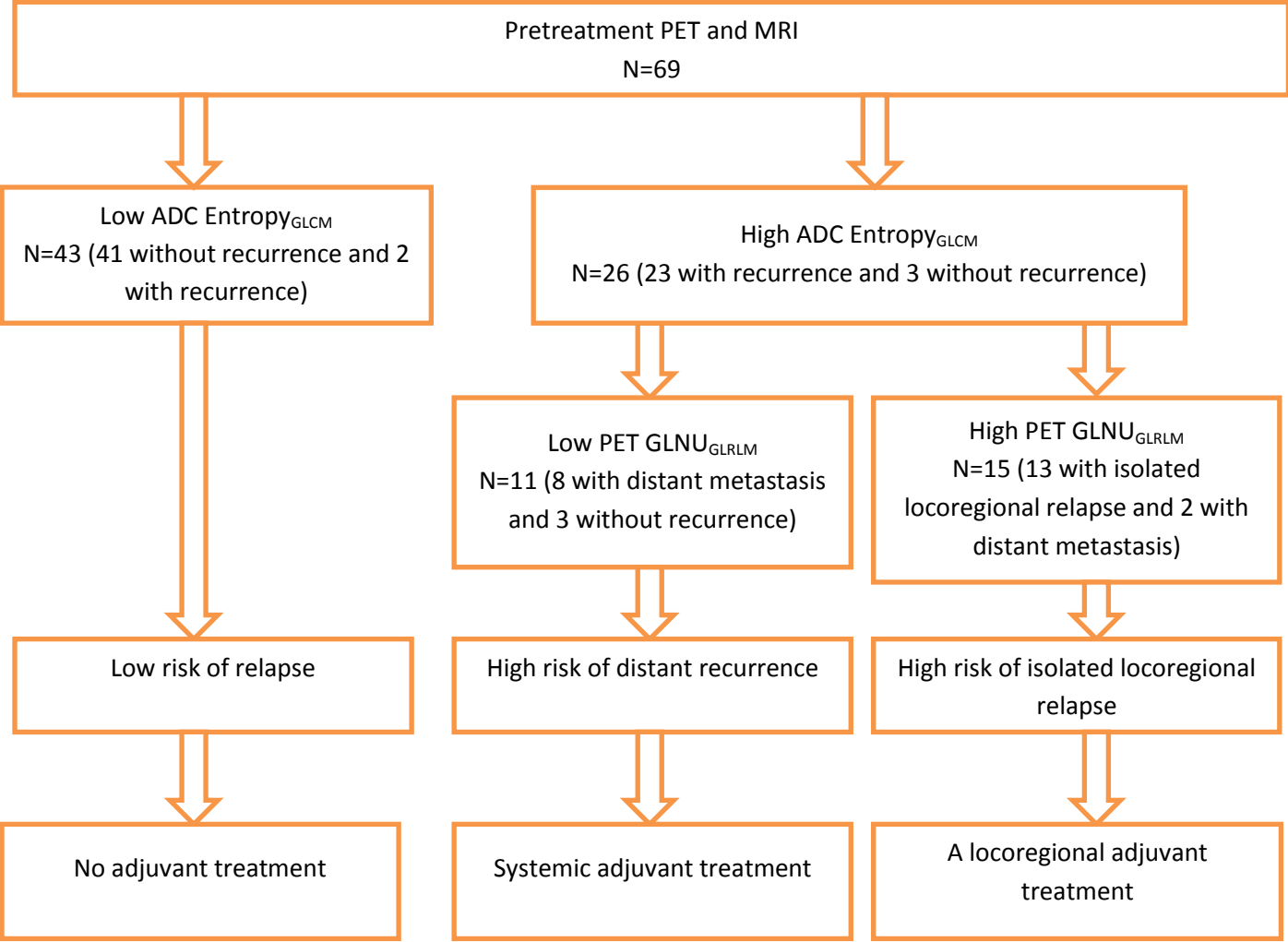


Figure 6: Flow diagram of risk-stratification strategy based on pretreatment FDG PET and DWI MRI illustrated in (A) the training set and (B) the testing set. The first step separates patients into two groups: low (first group) and high risk of relapse thanks to ADC Entropy_{GLCM} from DWI MRI. The second step further discriminates within the high-risk group between metastatic (second group) or pelvic (third group) relapse. The first group would not require additional treatment. The second group could benefit from a complementary systemic treatment, and the third group could be treated with an additional locoregional treatment (like surgery or additional boost in brachytherapy).

A



B

